Alma Mater Studiorum Università di Bologna
Archivio istituzionale della ricerca

Predicting the Second-Order Nonlinear Optical Responses of Organic Materials: The Role of Dynamics

(Article begins on next page)

23 February 2025

This is the final peer-reviewed accepted manuscript of:

F. Castet, C. Tonnelé, L. Muccioli, B. Champagne "Predicting the Second-Order Nonlinear Optical Responses of Organic Materials: the Role of Dynamics" *Acc. Chem. Res.* **55, 3716-3726 (2022)**

The final published version is available online at:
https://dx.doi.org/10.1021/acs.accounts.2c00616

Terms of use:

Predicting the Second-Order Nonlinear Optical Responses of Organic Materials: the Role of Dynamics

Frédéric Castet[1], Claire Tonnelé[2], Luca Muccioli[3], Benoît Champagne[4]

[1] Univ. Bordeaux, CNRS, Bordeaux INP, ISM, UMR 5255, F-33400 Talence, France. [2] Donostia International Physics Center (DIPC), Manuel Lardizabal Ibilbidea 4, 20018 Donostia, Euskadi, Spain. [3] Department of Industrial Chemistry ''Toso Montanari'', University of Bologna, Viale Risorgimento 4, 40136 Bologna, Italy. [4] Unité de Chimie Physique Théorique et Structurale, Chemistry Department, Namur Institute of Structured Matter, University of Namur, Rue de Bruxelles 61, 5000 Namur, Belgium.

CONSPECTUS GRAPHIC
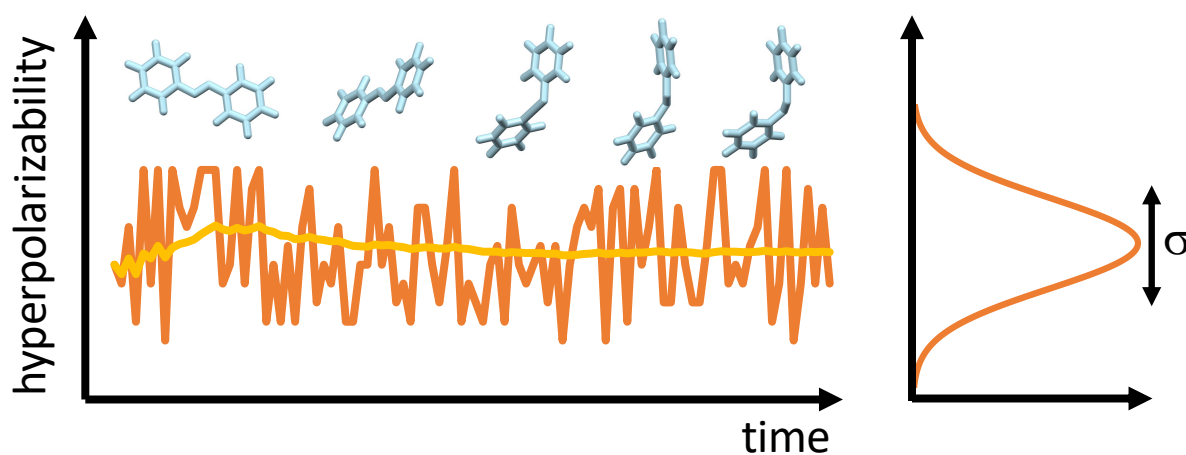
CONSPECTUS

The last thirty years have witnessed an ever-growing application of computational chemistry for rationalizing the nonlinear optical (NLO) responses of organic chromophores. More specifically, quantum chemical calculations proved highly helpful in gaining fundamental insights on the factors governing the magnitude and character of molecular first hyperpolarizabilities (β), be they either intrinsic to the chromophore molecular structure and arising from symmetry, chemical substitution or π-electron delocalization, or induced by external contributions such as the laser probe or solvation and polarization effects. Most theoretical reports assumed a rigid picture of the investigated systems, the NLO responses being computed solely at the most stable geometry of the chromophores. Yet, recent developments combining classical molecular dynamics (MD) simulations and DFT calculations have evidenced the significant role of structural fluctuations, which may induce broad distributions of NLO responses, and even generate them in some instances.

This account presents recent case studies in which theoretical simulations have highlighted these effects. The discussion specifically focuses on the simulation of the second-order NLO properties that can be measured experimentally either from Hyper-Rayleigh Scattering (HRS) or Electric-Field Induced Second Harmonic Generation (EFISHG). More general but technical topics concerning several aspects of the calculations of hyperpolarizabilities are instead discussed in the supporting information.

Selected examples include organic chromophores, photochromic systems and ionic complexes in the liquid phase, for which the effects of explicit solvation, concentration and chromophore aggregation are emphasized, as well as large flexible systems such as peptide chains and pyrimidine-based helical polymers, in which the relative variations of the responses were shown to be several times larger than their average values. The impact of geometrical fluctuations is also illustrated for supramolecular architectures through the examples of

nanoparticles formed by organic dipolar dyes in water solution, whose soft nature allows for large shape variations translating into huge fluctuations in time of their NLO response, and of self-assembled monolayers (SAMs) based on indolino-oxazolidine or azobenzene switches, in which the geometrical distortions of the photochromic molecules, as well as their orientational and positional disorder within the SAMs, again highly impact their NLO response and contrast upon switching. Finally, the effects of the rigidity and fluidity of the surrounding are evidenced for NLO dyes inserted in phospholipid bilayers.

Key References

- Pielak, K.; Tonnelé, C.; Sanguinet, L.; Cariati, E.; Righetto, S.; Muccioli, L.; Castet, F.; Champagne B. Dynamical behavior and second harmonic generation responses in acido-triggered molecular switches *J. Phys. Chem. C.* **2018**, *122*, 26160-26168.[1] *Simulations show how thermally-induced geometrical fluctuations, including the ion pair configuration, broaden the distributions of the SHG responses of indolino-oxazolidine acidochromic switches in solution, and rationalize the variations of these responses with respect to the closure/opening of the oxazolidine ring and to the nature of chemical substitution.*

- Tonnelé, C.; Champagne, B.; Muccioli, L.; Castet F. Nonlinear Optical Contrast in Azobenzene-Based Self-assembled Monolayers *Chem. Mater.* **2019**, *31*, 6759-6769.[2] *Calculations provide an atomistic picture of the morphology of azobenzene-based monolayers. They reveal a high degree of positional disorder of the chromophores, which significantly impacts the amplitude of the NLO responses of the materials, as well as of their contrast upon switching.*

- Bouquiaux, C.; Tonnelé, C.; Castet, F.; Champagne B. Second-Order Nonlinear Optical Properties of an Amphiphilic Dye Embedded in a Lipid Bilayer. A Combined

Molecular Dynamics - Quantum Chemistry Study *J. Phys. Chem. B* **2020**, *124*, 2101-2109.[3] *Calculations evidence the large enhancement of the second harmonic signal of an amphiphilic dye embedded in a lipid bilayer, which results both from the dynamical flexibility of the dye and from the electrostatic polarization due to the surrounding bilayer lipids.*

- Lescos, L.; Beaujean, P.; Tonnelé, C.; Aurel, P.; Blanchard-Desce, M.; Rodriguez, V.; de Wergifosse, M.; Champagne, B.; Muccioli, L.; Castet F. Self-assembling, structure and nonlinear optical properties of fluorescent organic nanoparticles in water *Phys. Chem. Chem. Phys.* **2021**, *23*, 23643-23654.[4] *The spontaneous formation and dynamical behavior of second harmonic scattering responses of amorphous nanoparticles based on organic dipolar dyes in water solution are rationalized by combining MD simulations and simplified DFT calculations explicitly accounting for intermolecular interactions.*

INTRODUCTION

The invention of lasers in 1960[5] was closely followed by the discovery of nonlinear optical (NLO) phenomena, such as the Second-Harmonic Generation (SHG) first demonstrated by Franken *et al.*[6] in crystalline quartz. Since then, SHG has proven to be a versatile tool for characterizing surfaces, interfaces and monolayers,[7,8] and has progressively become central to a broad range of applications in optical telecommunications, data storage, and signal processing.[9,10] Furthermore, the use of SHG in microscopy, first proposed by Sheppard *et al.* in 1977,[11] and the observation, a few years later, of a rat-tail tendon by a SHG microscope,[12] marked the birth of second harmonic imaging microscopy (SHIM)[13,14].

In this context, the design of materials exhibiting large SHG responses has been a continuous source of research in the past thirty years. Among others, organic compounds have attracted

particular interest due to advantages such as tailored synthesis and easy processing, as well as the possibility of realizing flexible devices with large and fast responses. Most systems reported to date are based on dipolar π-conjugated dyes incorporating strong electron-donor (D) and acceptor (A) groups connected through a π-conjugated bridge. Their first hyperpolarizability (β) can be tuned by varying the nature of the D/A substituents, as well as the length and planarity of the bridge.[15] Also symmetry can be exploited to modulate the magnitude of the NLO responses, as exemplified by the high β values reported for V-shape dipolar chromophores[16] and octupolar systems.[17,18,19] The potential use of NLO systems as sensors or active components in optoelectronic and photonic devices such as logic gates or high-density optical memories has motivated many recent works.[20,21,22,23,24,25,26] In these applications, an important figure of merit is the β contrast between the different forms generated by controlled chemical conversions, for instance with light irradiation at specific frequencies, by applying a redox potential, or by varying pH and temperature. Large response variations can also be triggered by a change in the supramolecular complexation, a feature that can be exploited for environmental monitoring.

The quest for new NLO materials usually relies on complementary experimental and theoretical approaches. Quantum chemical calculations are highly helpful to understand the factors governing the magnitude and character of molecular hyperpolarizabilities, and to disentangle the effects intrinsically linked to the molecular structure from those arising from the environment or the experimental setup. Owing to its computational efficiency, (time-dependent) Density Functional Theory, (TD)-DFT, has rapidly become the method of choice for investigating real-life molecules, for which calculations with correlated wavefunction methods often remain prohibitive.[27,28,29,30,31,32,33] However, most theoretical studies rely on the assumption that the investigated systems are rigid in nature, with the NLO responses being computed on at most a few, but generally just one single geometry of the chromophores.

Although this choice is usually well-grounded for obtaining a qualitative description of the NLO properties, our recent studies combining classical molecular dynamics (MD) simulations and DFT calculations, backed up by experimental observations, have evidenced the significant role of structural fluctuations. Indeed, dynamic disorder may induce broad time fluctuations of NLO responses and even, in some cases, be at their origin. In this Account we discuss a suitable computational strategy to include dynamic effects and we elucidate their impact on the Hyper-Rayleigh Scattering (HRS) and Electric Field-Induced Second Harmonic Generation (EFISHG) responses for a few selected systems of increasing complexity.

2. EXPERIMENTAL OBSERVABLES

At the molecular scale, the linear and nonlinear optical properties are defined by the equation describing the influence of external electric fields on the dipole moment. The ζ-cartesian component of the induced dipole reads:

$$\Delta\mu_\zeta(-\omega_\sigma) = \alpha_{\zeta\eta}(-\omega_\sigma;\omega_1)E_\eta(\omega_1) + \frac{1}{2}\beta_{\zeta\eta\chi}(-\omega_\sigma;\omega_1,\omega_2)E_\eta(\omega_1)E_\chi(\omega_2) +$$

$$\frac{1}{6}\gamma_{\zeta\eta\chi\xi}(-\omega_\sigma;\omega_1,\omega_2,\omega_3)E_\eta(\omega_1)E_\chi(\omega_2)E_\xi(\omega_3) + \cdots \tag{1}$$

where $\alpha_{\zeta\eta}$, $\beta_{\zeta\eta\chi}$, and $\gamma_{\zeta\eta\chi\xi}$ are elements of the polarizability (α), the first (β), and the second (γ) hyperpolarizability tensors expressed in molecular frame cartesian coordinates, η, χ and ξ. Each term represents an induced dipole oscillating at a different frequency $\omega_\sigma = \omega_1 + \omega_2 + \cdots$ for a specific set of electric fields, $E_\eta(\omega_1), E_\chi(\omega_2), \dots$ polarized along the $\eta, \chi, \dots$ molecular axes, and oscillating at angular frequencies $\omega_1, \omega_2, \dots$; the summations over repeated indices are assumed.

This Account deals with the second-order SHG response associated with $\beta(-2\omega;\omega,\omega)$, and with the third-order EFISHG phenomenon, described by $\gamma(-2\omega;\omega,\omega,0)$. The former can be probed by using the HRS technique.[34] In typical HRS experiments, the vertically-polarized scattered light is collected at an angle of 90° with respect to the incident light direction and the

scattered intensity is proportional to $\beta_{HRS}^2(-2\omega; \omega, \omega)$, which contains two terms, $\langle\beta_{ZZZ}^2\rangle$ and $\langle\beta_{ZXX}^2\rangle$, associated to vertically- and horizontally-polarized incident light in the XYZ laboratory frame:

$$\beta_{HRS}(-2\omega; \omega, \omega) \equiv \beta_{HRS} = \sqrt{\langle\beta_{ZZZ}^2\rangle + \langle\beta_{ZXX}^2\rangle} \tag{2}$$

The full expressions of $\langle\beta_{ZZZ}^2\rangle$ and $\langle\beta_{ZXX}^2\rangle$ in function of the molecular components of the β tensor are given in SI. Conversely, when employing the EFISHG setup, the SHG response contains both a β and a γ contribution:[35]

$$\gamma_{EFISHG} = \gamma_{//}(-2\omega; \omega, \omega, 0) + \frac{\mu_0\beta_{//}(-2\omega;\omega,\omega)}{3kT} \tag{3}$$

Though for push−pull π-conjugated compounds the $\gamma_{//}$ term is usually negligible, measurements at several temperatures are in principle required to disentangle the second- and third-order responses, besides the norm μ_0 of the permanent dipole moment is also needed to access $\beta_{//}$.[36]

The SHG response of a surface is described by its macroscopic second-order NLO susceptibility, $\chi^{(2)}$, which can be understood as an effective β per unit surface:

$$\chi_{XYZ}^{(2)}(-2\omega; \omega, \omega) = \frac{N_s}{\varepsilon_0} \sum_{\zeta\eta\chi} \langle T_{X\zeta Y\eta Z\chi}(\phi, \theta, \xi)\, \beta_{\zeta\eta\chi}^{eff}(-2\omega; \omega, \omega)\rangle \tag{4}$$

where N_s is the molecular surface density, $T_{X\zeta Y\eta Z\chi}(\phi, \theta, \xi)$ is the rotation matrix between the laboratory and molecular coordinate systems (related through the Euler angles ϕ, θ, and ξ), and the $\langle...\rangle$ bracket accounts for the average over the azimuthal angle θ, as well as for reflection symmetries in the case of achiral surfaces. When β calculations are performed on a sufficiently large number of uncorrelated snapshots produced by MD simulations, these averages are implicit. Depending on the polarization p (in the plane of incidence) or s (perpendicular to this plane) of the incident and reflected lights, different combinations of $\chi_{XYZ}^{(2)}$ tensor components and therefore of $\beta_{\zeta\eta\chi}^{eff}$ tensor components are probed. The latter is denominated "effective" because it is not that of the isolated chromophore, but it includes polarization, dispersion, and

exchange-overlap effects originating from its surrounding, sometimes referred to as ''dressing'' effects. Most studies target only the dominant $\chi^{(2)}$ contributions, typically $\chi^{(2)}_{ZZZ}$ or its sum with $\chi^{(2)}_{ZXX}$ and $\chi^{(2)}_{ZYY}$, where Z is the normal to the surface.

3. COMPUTATIONAL STRATEGY

The high computational cost of correlated wavefunction methods and ab initio molecular dynamics (AIMD) makes such approaches prohibitive for considering environment and dynamic effects in the evaluation of NLO responses. A cost-effective alternative consists in treating these effects with classical mechanics and decoupling them from the Quantum Mechanics (QM) calculation of the NLO properties. As illustrated in Figure 1, several strategies have been developed for this purpose: the simplest one consists in performing calculations on Maxwell-Boltzmann-weighted (MB) ensembles of conformers, while more sophisticated schemes rely on Rigid-Body Monte-Carlo (MC) or atomistic Molecular Dynamics (MD). So far, the MD+DFT combination, which in principle can catch both intra- and intermolecular vibrational effects (see discussion on the vibrational contributions in SI), is the most satisfactory option. As discussed at greater length in the SI, the accuracy of this approach however relies i) on the quality of the force field employed in the MD simulations, which should be able to finely reproduce relevant structural features (bond length alternation, conformations, specific intermolecular interactions such as H-bonds) that strongly affect the NLO response, and ii) on the quality of the sampling to extract reliable averaged properties. Obviously, the level of approximation used for computing the NLO properties is also of key importance, as well as the way polarization effects from the environment are taken into account, and, as recently put forward, also quantum repulsion effects between the chromophore and the environment.[37] As schematized in Figure 1, these latter can be described at different

degree of complexity, either using a Polarized Continuum Model (PCM), through electrostatic embedding (EE, including Point Charge Embedding (PCE) with fixed charges or more refined polarizable schemes), or using explicit QM (see SI).

Dynamic effects

| Single geometry (QM) | Maxwell-Boltzmann average (QM-MB) | Rigid-Body Monte-Carlo (RB-MC) | Molecular dynamics (MD) |

Lowest-energy structure
no dynamical effects

Weighted sum of few conformers
static molecular distortions

Set of uncorrelated snapshots
dynamic positional disorder

Set of uncorrelated snapshots
dynamic positional disorder and molecular distortions

Environment effects

| Gas phase (none) | Polarizable Continuum Model (PCM) | Electrostatic Embedding (EE) | Explicit environment (sTD-DFT) |

Isolated molecule
no environment effects

Implicit environment
polarization effects

Electrostatic environment
system-specific polarization effects

Full quantum calculation
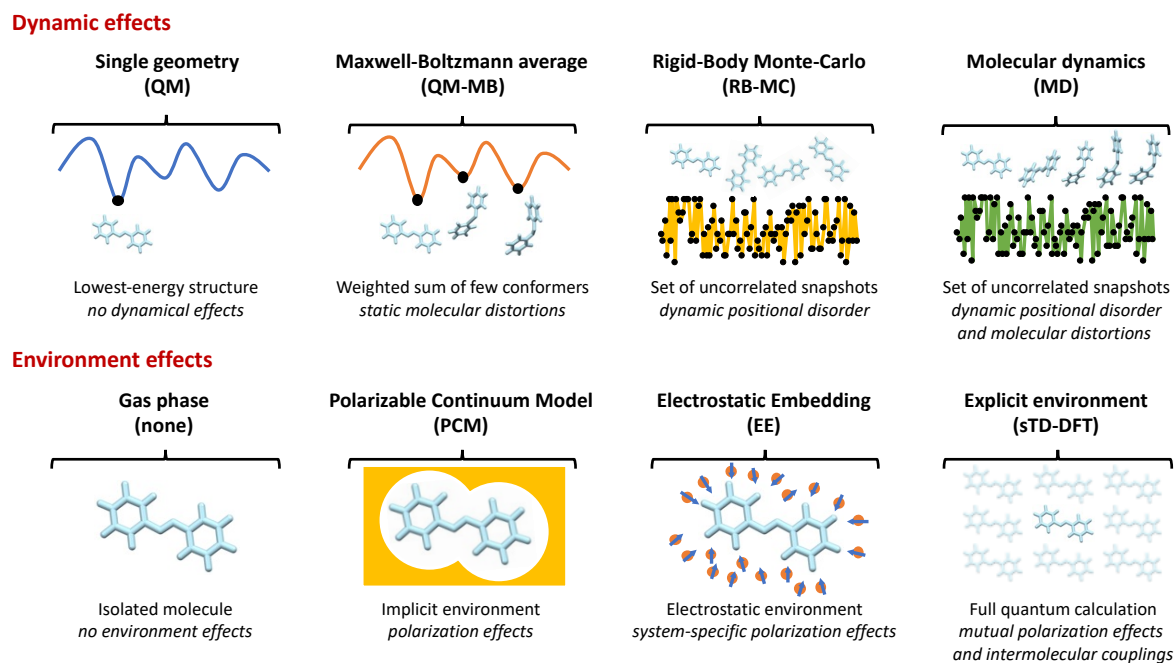*mutual polarization effects and intermolecular couplings*

Figure 1: Sketch of the different methods used for describing structural fluctuations and environment effects in the calculation of NLO properties.

Owing to the size of the QM region (the chromophore and the necessary surrounding molecules or ions), and to the number of snapshots required for an adequate sampling, the range of first principles methods to calculate β is in practice restricted to (TD)-DFT and the related quadratic response methods.[38] The task becomes therefore to find reliable exchange-correlation (XC) functionals. The selection of XC functionals and their validations are discussed in details in SI, emphasizing i) on the intrinsic nonlocal character of the hyperpolarizabilities because these are responses to electric fields, ii) on the subsequent role of Hartree-Fock exchange and the different ways to include it, iii) on the high-level electron correlation methods used for benchmarking DFT approximations, iv) on the description of the frequency dispersion of β, as well as v) on simplified TD-DFT schemes (sTD-DFT),[39] which can be applied to systems

containing hundreds or thousands of atoms, therefore explicitly accounting for aggregation and other surrounding effects.

4. CASE STUDIES

4.1. Dyes in solution

The MD+QM scheme described above was largely employed to characterize the SHG response of various organic species in solution (see Table SI2). As a first representative example we select the molecular switches **1** and **2** displayed in Figure 2a, resulting from the association of an indolino-oxazolidine switchable unit with a bithiophene donor. In acetonitrile or chloroform solutions, the addition of trifluoroacetic acid triggers the switching from a neutral closed form to a protonated open form (POF) that makes an H-bonded ion pair with the trifluoroacetate counterion. The opening of the indolino-oxazolidine ring enables π-electron delocalization between the bithiophene and indoleninium moieties, which in turn induces a strong enhancement of the SHG response.

For these systems, DFT-MB calculations reproduced the large increase of β observed with HRS measurements upon acid addition in acetonitrile. They also helped rationalizing the smaller β_{HRS} contrast observed for the nitro-substituted derivative compared to the methylated one, originating from the exaltation of the HRS response of the closed form by the nitro group.[40] However, although accounting for the conformer population improves the comparison with experimental results with respect to estimates solely based on the most stable conformer, the β(open)/β(closed) ratios were still significantly overestimated (Figure 2d, "DFT" data). This discrepancy turned out to be independent of the XC functional, and MP2 calculations did not allow a better agreement with the experiment.

The agreement instead improves drastically when accounting for the dynamic behavior of the molecular switches at MD+QM level, in which the interactions between the POFs and the

trifluoroacetate ion were also treated explicitly in DFT calculations.[1] As illustrated in Figure 2c for compound **2**, the thermally-induced fluctuations in the geometry of the chromophores and the mobility of the counterion lead to large standard deviations of the HRS response. The average β_{HRS} for the POF/trifluoroacetate ion pair is about 40% smaller than that computed using the DFT-MB approach without the counterion, while the β_{HRS} of the closed form is decreased by ~10%. A similar trend is found for compound **1**. Therefore, the computed β contrasts are significantly lowered and get much closer to the experimental ones (Figure 2d, "MD+DFT" data). Dynamic effects have an even more crucial impact on the EFISHG responses of these systems, whose measurements were made possible owing to the electric neutrality of AC pairs formed, in chloroform, by the POF and the trifluoroacetate anion.[1] Remarkably, for both forms of compound **1**, standard deviations on $\beta_{//}$ were shown to be several times larger than their corresponding averages, making difficult even the determination of their sign. Moreover, MD+QM calculations revealed an almost perfect orthogonality between the vectorial component of β and the dipole moment for the POF of compound **1**, cancelling out the second-order contribution and making the third-order term, usually neglected in data analysis, dominant in equation (3). Note that in this work, the DFT-MB approach was not considered to describe the properties of the POF/trifluoroacetate AC pair. In most cases, the latter scheme can be applied only to single molecules with well-defined conformations, otherwise the potential energy surface (PES) becomes too complex to be fully sampled with QM energy minimizations. Boltzmann sampling could nevertheless be suitable when strong directional interactions (e.g. hydrogen bonds) exist between the two ions, since the latter constrain the structure and reduce the complexity of the PES.
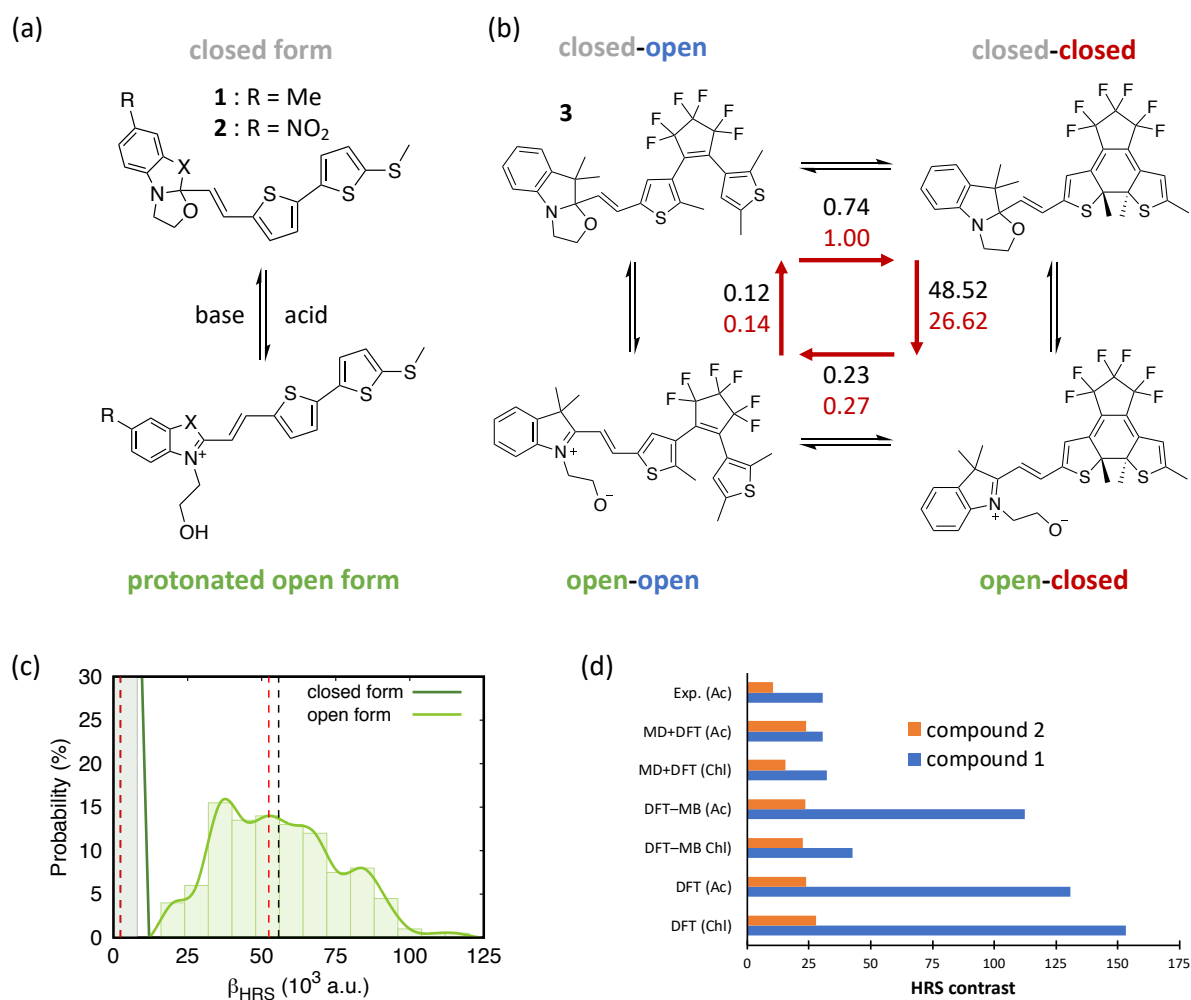
Figure 2: (a) Closed form (CF) and protonated open form (POF) of indolino-oxazolidine derivatives **1** and **2**; (b) Interconversion scheme for biphotochromic switch **3**, with β_{HRS} contrasts computed using the IEF-PCM/HF (black) and MD+QM(HF) (red) levels using an incident wavelength of 1907 nm; (c) Distributions and averages of dynamic (1907 nm) β_{HRS} values of compound **2** computed with the MD+QM(DFT) scheme (black vertical lines) and with the DFT-MB approach (red vertical lines) in acetonitrile; (d) β_{HRS} contrasts upon CF $\rightarrow$ POF switching in compounds **1** and **2** calculated in acetonitrile (Ac) and chloroform (Chl).

The influence of solvent interactions on the HRS responses of the different forms of the biphotochromic switch **3** (Figure 2b) in acetonitrile was assessed using either an implicit model (IEF-PCM) or an explicit PCE, in which solvent charge positions were generated by RB-MC

simulations.[41] These calculations allowed to specifically address the impact of fluctuations in the solvent polarization field due to the motion of solvent molecules, while excluding the effects of dynamical distortions of the chromophores. They evidenced that β_{HRS} calculated using IEF-PCM are usually larger than those obtained with the RB-MC approach. However, both models predicted similar contrasts (Figure 2b), indicating that implicit solvation schemes are suitable to describe solvent effects on the NLO responses of molecular switches.

The RB-MC+QM computational strategy was also applied for predicting the effect of nitrobenzene concentration in nitrobenzene/benzene binary solutions.[42,43] When only one reference nitrobenzene molecule is contained in the QM part, β_{HRS} and $\beta_{//}$ both increase steadily with nitrobenzene concentration, due to the growing polarization field created by the point charges of polar nitrobenzene molecules in the MM region. However, when the first solvation shell is considered explicitly in the QM region, the NLO response per nitrobenzene molecule instead largely decreases at increasing nitrobenzene concentration, as a consequence of the electrostatic interactions between nitrobenzene molecules and of their partial centro-symmetric arrangements. These results point out the crucial importance of the definition and the shape of the QM region, as further discussed in sections 4.3 and 4.4, as well as the need for polarizable environments.

The challenge of including solvent polarization effects in the calculation of NLO properties was also tackled by means of QM/MM based methods, in which a polarizable embedding was introduced in the MM part through fluctuating charges. This approach makes the solvent electrostatic potential in the MM part responding self-consistently to the electrostatic potential of the QM moiety through the introduction of point charges that fluctuate according to differences in atomic electronegativities. This strategy was recently coupled to classical MD simulations in order to evaluate the HRS response of organic acids in aqueous solution.[44] In an alternative scheme, the polarization due to the surrounding solvent molecules was included via

14

a self-consistent local field that is determined from the interactions between the molecular multipoles and their polarizabilities, which were evaluated beforehand at QM levels.[45] This electrostatic dressing field (and its gradient) was combined with classical MD simulations employing either non-polarizable or polarizable force fields, and used to evaluate the EFISHG and HRS properties of the para-nitroaniline molecule in cyclohexane, tetrahydrofuran and 1,4-dioxane solutions. The macroscopic susceptibilities were subsequently evaluated from the molecular responses, using classical electrostatic interactions schemes. These studies further demonstrated that the reliable prediction of NLO properties of solvated molecules requires using both representative sets of geometries and polarizable environments for the simulation of the liquid structure.

4.2. Polymers and peptide chains

Dynamic structural effects are particularly significant in the case of large flexible structures such as polymeric strands, as demonstrated in an early work for pyridine-pyrimidine and hydrazone-pyrimidine foldamers (Figures 3a and 3b).[46] Combining classical conformational samplings in vacuum using the MMFF94 force field and TD-HF calculations, it was demonstrated that geometrical fluctuations are responsible for relative variations of ∼20% in the HRS responses in both structures. As for small molecules, EFISHG responses were shown to be even more sensitive to dynamic disorder, with variations reaching up to five times their mean value. In the same spirit, a more recent study reported the role of disorder on the SHG responses of tryptophane-rich model peptides (Figure 3c and 3d).[47] Here, the potential energy surface in water was sampled using a meta-dynamics approach with an implicit solvation model and the tight-binding-based GFN2-xTB Hamiltonian.[48] First hyperpolarizabilities were calculated using the sTD-DFT-xTB method, which enables computations for systems with up to several thousands of atoms. Structure-property analyses revealed a correlation between the magnitude of β_{HRS} and the relative orientations of indole moieties in the tryptophan sequence,

with strongly enhanced values when indole dipoles are aligned parallel to each other. This study thus evidenced the importance of carefully exploring the conformational space of flexible chromophores, as well as all the possible chromophore orientations, for achieving reliable NLO calculations.
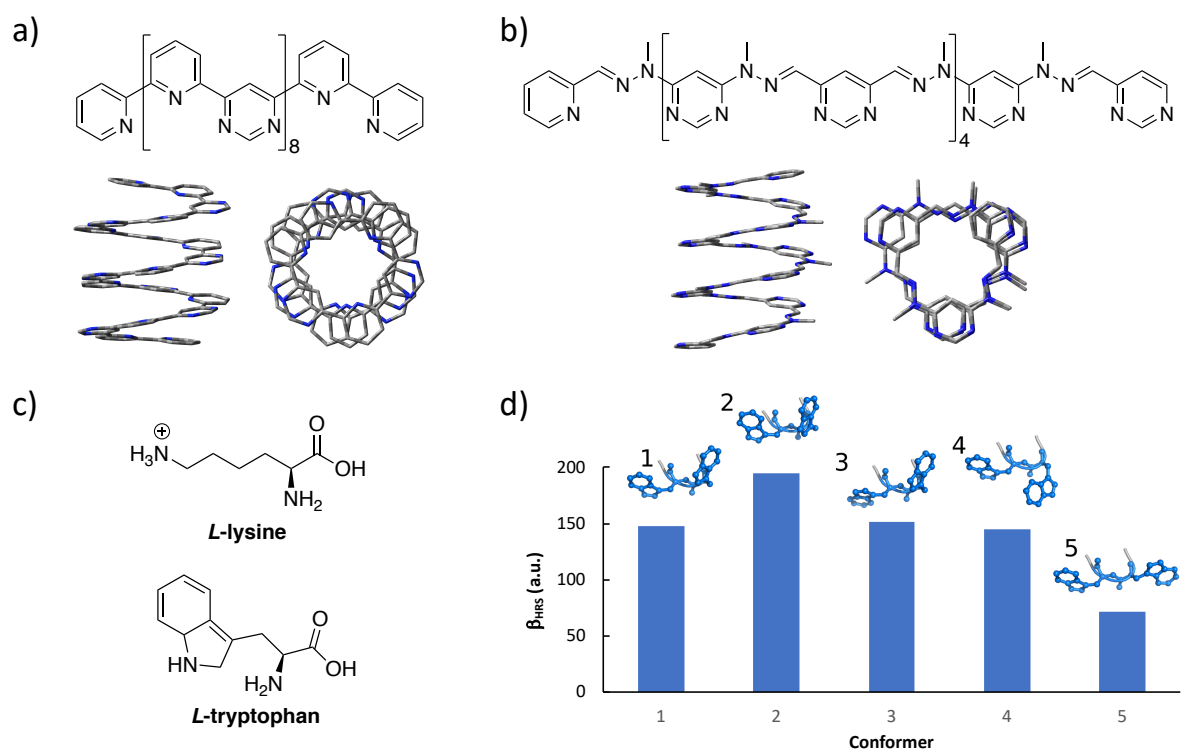

Figure 3: a) Structure of pyridine-pyrimidine and b) hydrazone-pyrimidine foldamers; c) Lewis structures of lysine and tryptophan amino acids; d) β_{HRS} of the five more stable conformers of the KWWK model peptide in water, where W and K denote tryptophan and lysine units, respectively. Figs. 3a-b adapted from Ref. 46. Copyright 2009 American Chemical Society.

4.3. Aggregation effects

The sensitivity to dynamic disorder is also key in complexes involving weakly interacting subunits. The first investigation of conformational dynamic effects was carried out, as early as 1998, by Kenis *et al.*[49], on a multichromophoric calix[4]arene system. However, for this rather

rigid system, the effects on the β_{HRS} responses of its four conformers are small, with averaged values closely matching those obtained on the structures optimized at the MM/CHARMm level. More recently, the impact of anion-cation (AC) interactions on EFISHG was systematically investigated for ion pairs involving the stilbazolium cation and anions of different nature (Figure 4a).[50] MD+QM calculations revealed that the EFISHG response is dominated by its second-order contribution, and confirmed that the relative amplitudes of $\gamma_{//}$ and $\mu_0\beta_{//}/3kT$ in γ_{EFISHG} are linked to the position of the anion with respect to the charge-transfer axis of the stilbazolium, which determines the angle between the dipole moment and β vectors (Figure 4b). These investigations were further extended to include the effects of chromophore aggregation.[51] MD simulations demonstrated that AC pairs have a strong propensity to self-aggregate at high-concentration, and to form stable $(AC)_2$ dimers adopting mainly Λ and head-to-head shapes. Owing to the increased centrosymmetric character of $(AC)_2$ aggregates compared to single AC pairs, aggregation significantly lowers the average EFISHG response. Only considering the simultaneous presence of AC and $(AC)_2$ structures eventually allowed to reproduce and interpret the experimental trends.

A step further towards the accurate description of NLO properties of large molecular aggregates was achieved in a recent MD+QM study of the HRS response of amorphous nanoparticles formed by organic dipolar dyes in water (Figure 4d).[4] MD simulations allowed rationalizing the spontaneous formation of the nanoparticles, as well as the onset of polar π-stacked domains at the water interface.[52] They also evidenced that the soft nature of the nanoparticles allows for rather large shape variations (Figure 4c), which translate into large time fluctuations of their NLO response. Performing QM calculations using the valence-MO tight-binding variant of the sTD-DFT scheme (sTD-DFT-vTB) enabled accounting for mutual polarization effects of the dyes at a full quantum level and highlighted the key role of intermolecular interactions on the HRS response. The latter are at the origin of the emergence

of low-lying excited states that are responsible for the appearance of a red shifted tail in the linear absorption spectrum (Figure 4e) and, entering into resonance with the second harmonic light, for the large enhancement of the HRS signal observed experimentally upon aggregation.
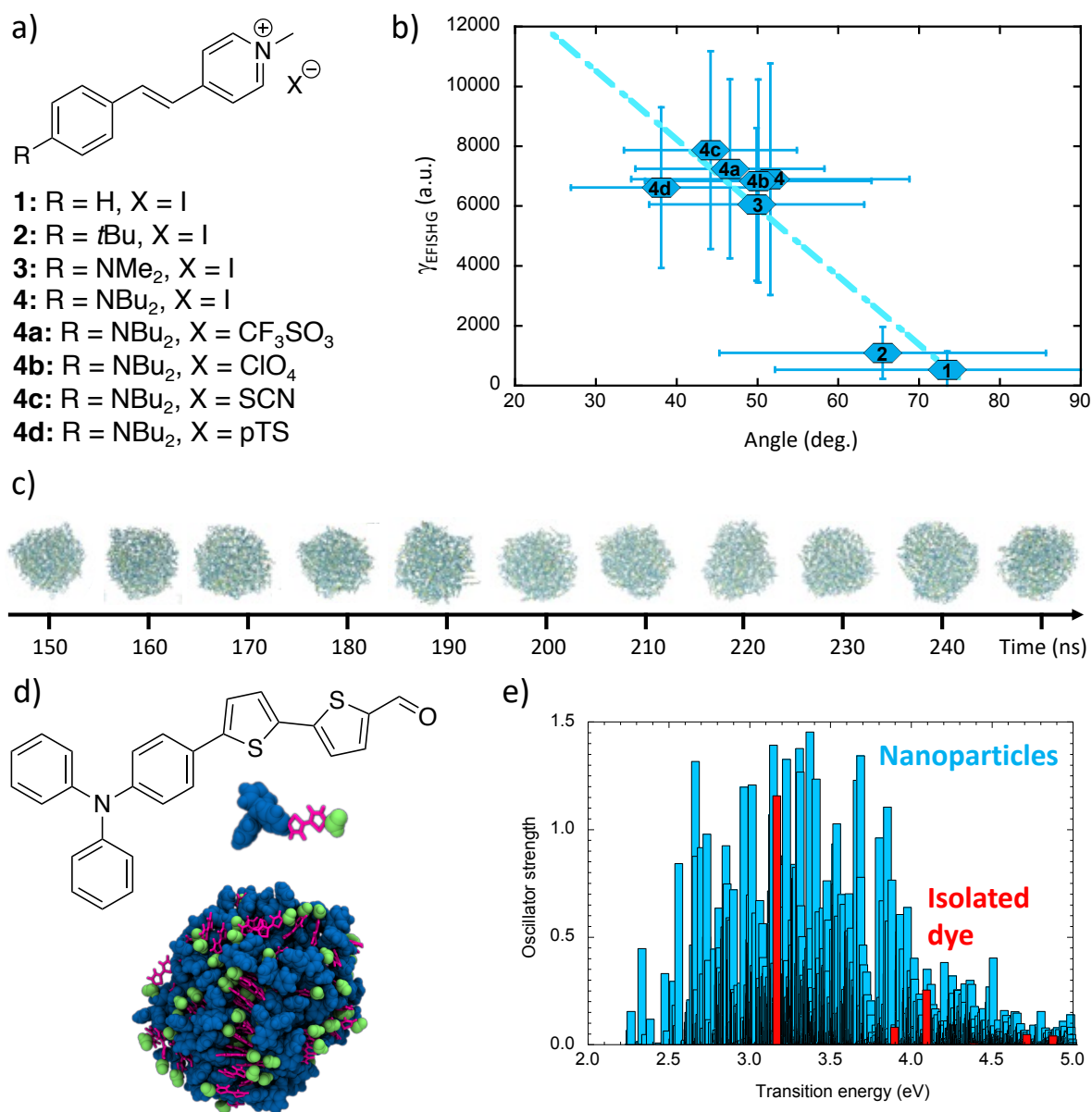

Figure 4: a) Structure of the stilbazolium cations with various anions; b) Evolution of γ_{EFISHG} (equation 3) as a function of the angle between the dipole and hyperpolarizability vectors for the anion/cation series of scheme 4a; c) Snapshots picturing the time evolution of a nanoparticle shape along a MD trajectory; d) Structure of the isolated dipolar dye and of a supramolecular

aggregate formed of 100 dyes; (e) dominant electronic transitions in a nanoparticle (blue bars) and in the isolated dye (red bars) calculated at the sTD-DFT-vTB level. Figs. 4c-e adapted from Ref. 4. Copyright 2021 Royal Society of Chemistry.

4.4. Self-assembled monolayers

By constraining the alignment of the molecular units at controlled concentrations, surface coating with self-assembled monolayers (SAMs) constitutes an efficient strategy for introducing NLO chromophores into a device to maximize its macroscopic SHG response and/or contrast. In this context, the MD+QM approach was used to investigate the dynamic behavior and NLO properties of photoresponsive SAMs constituted of organic photoswitches grafted onto amorphous SiO$_2$ surfaces. In a first study focusing on indolino-oxazolidine derivatives (Figure 5a),[53] MD simulations revealed that the photoresponsive moieties of the SAMs exhibit a high degree of orientational and positional disorder due to the flexibility of the thioalkyl anchoring group. Quite interestingly, DFT calculations carried out on a large selection of individual chromophores evidenced that, despite the large geometrical distortions and the lack of orientational order, the SHG contrast upon photochromic conversion in these SAMs is of the same order of magnitude as that of the corresponding molecule in solution. It was also demonstrated that despite the lack of structural order, chromophores in the SAM can only adopt a limited number of specific conformations due to the high rotational barriers around the chemical bonds of the conjugated skeleton. As already mentioned, a notable exception is the rotation about the thiophene–thioalkyl bond, which is not only almost free, but also strongly correlated with the magnitude of the first hyperpolarizability (Figure 5b). Controlling this rotation by chemical design thus offers a viable strategy to optimize the SHG response of photo-responsive devices based on indolino-oxazolidine SAMs.

In a second work, the same computational strategy was applied to investigate the morphologies and NLO response of azobenzene-based SAMs (Figure 5c) with different surface densities.[2] Here, distinct FF parameters were employed to describe the torsional potential around the azo junction in the ground and first excited state and exploited in a simulation scheme adapted to induce the *trans→cis* photoisomerization. These simulations suggested that when increasing the chromophore concentration, the steric hindrance reduces the *trans→cis* photoisomerization yield. Moreover, for all-*trans* SAMs, the first hyperpolarizability vector component normal to the surface plane (β_Z, equation S4) increases significantly with the packing density (Figure 5d) and is larger than the parallel one, in agreement with polarization-resolved SHG measurements.[54] In addition, the β contrast observed upon photoisomerization strongly depends on the chromophore concentration: the computed variations of β_Z range between 30% and 50% depending on the relative surface coverage (Figure 5e), in qualitative agreement with experimental data. Finally, although calculations on isolated molecules provide reasonable estimates of the photo-induced β contrast, further tests showed that introducing an electrostatic embedding allows capturing substantial variations in the anisotropy of the NLO response of densely packed aggregates (Figure 5e), improving the agreement with experimental data.
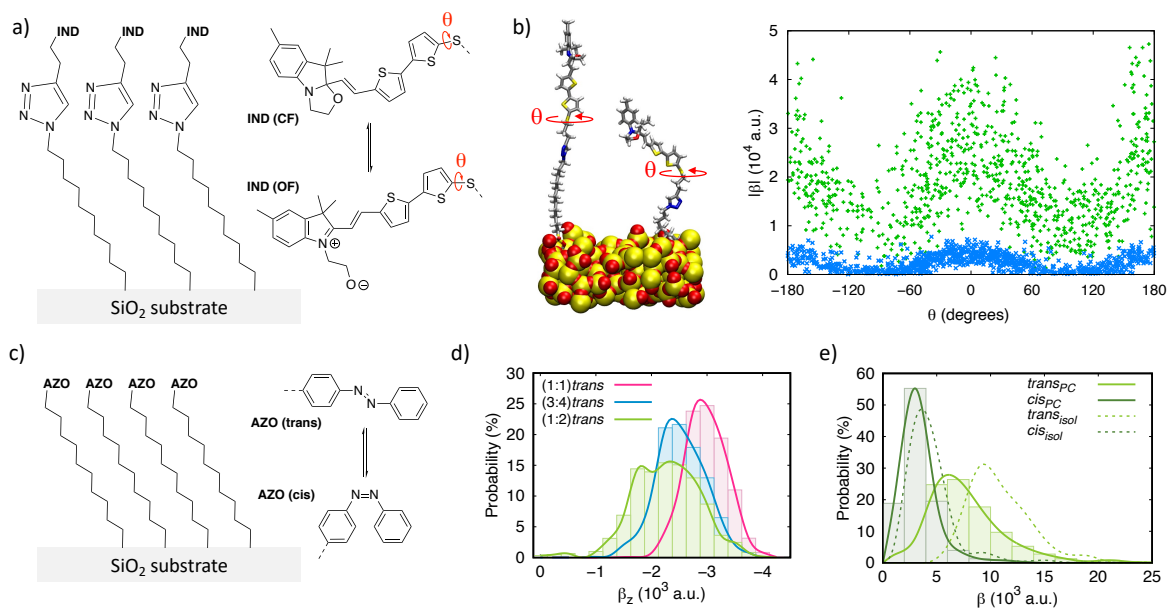
Figure 5: a) Sketch of a SAM based on indolino-oxazolidine (IND) photoswitches; b) β values plotted versus the θ torsion angle in closed (blue) and open (green) forms; c) Sketch of a SAM based on azobenzene (AZO) photoswitches; d) Distributions of the $\beta_Z(0)$ values in all-*trans* SAMs at different (*x:y*) surface coverages, with *x* the relative number of AZO-functionalized alkyl chains and *y* the total of functionalized and non-functionalized alkyl chains; e) Distributions of the $\beta(2\omega)$ values for *trans* and *cis* SAMs at (1:2) coverage, considered isolated (isol) or within a PC embedding. Figs. 5a-b adapted from Ref. 53. Copyright 2018 Royal Society of Chemistry. Figs. 5c-e adapted from Ref. 2. Copyright 2019 American Chemical Society.

4.5. SHG probes embedded in lipid bilayers

Finally, MD+QM schemes were also employed to investigate the NLO signals of exogenous dyes embedded in biological media. The investigated systems consisted in an aminonaphtylethenylpyridinium dye (ANEP, Figure 6a) inserted into glycerophospholipid phosphatidylcholine (PC) lipid membranes (Figure 6b). The results evidenced a significant

enhancement of β induced by the interactions of the dye with the lipid bilayer. These effects originate both from the flexibility of the chromophore and from the polarization of the surrounding, simulated using a PCE scheme.[3] The calculations were further extended to investigate the influence of cholesterol concentration on ANEP SHG response.[55] They showed that the progressive rigidification of the membrane, observed upon increasing the cholesterol molar fraction, increases the orientational order of the lipid molecules and the alignment of the charge transfer axis of ANEP with the bilayer normal, with a consequent enhancement of β_{ZZZ}^{eff} (Figure 6c). Therefore, the magnitude of the NLO response of the embedded dye can serve as probe of the composition-dependent orientational order of a bilayer or even more interestingly, of cell membranes.
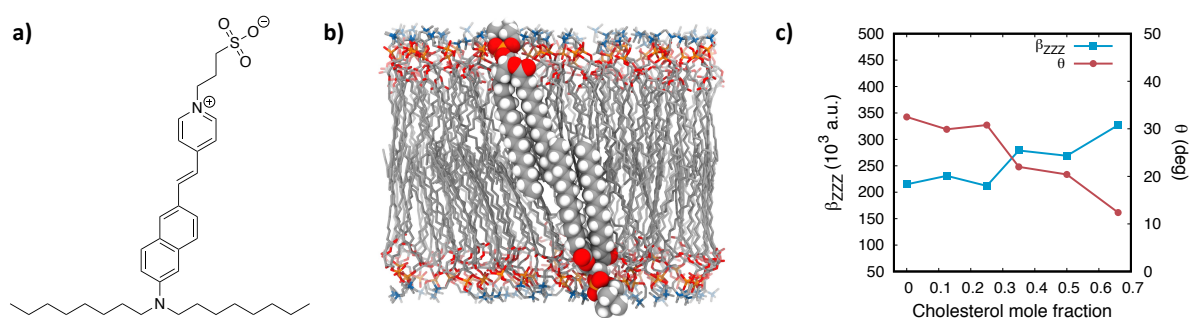

Figure 6: Structure of the ANEP dye (a) and of a phosphatidylcholine lipid membrane (b); (c) Evolution of β_{ZZZ}^{eff} and of the tilt angle characterizing the alignment of the dye with the bilayer normal as a function of cholesterol mole fraction. Fig. 6c adapted from Ref. 55. Copyright 2021 American Chemical Society.

5. CONCLUSIONS

The case studies discussed in this account demonstrate the striking role of dynamic fluctuations and structural order in the NLO response of conjugated organic molecular and supramolecular

systems. The sequential application of classical MD and DFT calculations constitutes a straightforward way to include these effects and enables accurate prediction of the targeted properties. However, this computational strategy requires the development of system- and property-specific force fields, which may limit its broad and systematic application. Future improvements should be oriented towards the development of fully integrated computational solutions, the ultimate (and still out of reach) scheme being ab initio molecular dynamics including on-the-fly calculations of the optical properties. This approach would also enable to take into account spatial correlations between molecules, an effect important for liquids as well as for concentrated solutions, which leads to a coherent contribution to the HRS response.[56] A promising step toward this objective might be found in introducing the quantum treatment of chromophore vibrations in the dynamics, for instance with semi-classical path integral methods.[57,58]

Another important aspect for accurate prediction of NLO responses of embedded probes lies in the description of the surrounding, which should at least allow for the possibility of delocalized excited states and mutual polarization effects. While the latter can be accurately treated with classical schemes such as classical electrostatics and polarizable force fields,[59,60] the former require a quantum treatment. Tractable strategies have been afforded by recently developed simplified time-dependent DFT schemes.[61,39] However, these methods also rely on semi-empirical parameters that need to be specifically adjusted for the investigated systems. The ongoing development of a new generation of sTD-DFT schemes, involving a reduction of the number 2-electron integrals based on the Zero Differential Overlap approximation and getting rid of the tedious parameter optimization, will certainly allow better transferability to the methodology. Quadratic response methods based on linear scaling DFT are also appealing alternatives.[62]

ASSOCIATED CONTENT

Supporting Information

Expressions for $\langle\beta_{ZZZ}^2\rangle$, $\langle\beta_{ZXX}^2\rangle$, $\gamma_{//}$, and $\beta_{//}$ in the molecular frame; discussion about the convergence of hyperpolarizabilities obtained with the MD+QM approach; presentation of key methods for modeling the effects of the surrounding; presentation of first principles methods to calculate the hyperpolarizabilities as well as of reliable DFT-based approximations; overview of theoretical studies employing sequential MD+QM calculations for evaluating NLO responses.

Author Information

Corresponding Authors

Frédéric Castet, *Univ. Bordeaux, CNRS, Bordeaux INP, ISM, UMR 5255, F-33400 Talence, France*. ORCID: 0000-0002-6622-2402; Email: frederic.castet@u-bordeaux.fr

Claire Tonnelé, *Donostia International Physics Center (DIPC), Manuel Lardizabal Ibilbidea 4, 20018 Donostia, Euskadi, Spain*. ORCID: 0000-0003-0791-8239; Email: claire.tonnele@dipc.org

Luca Muccioli, *Department of Industrial Chemistry ''Toso Montanari'', University of Bologna, Viale Risorgimento 4, 40136 Bologna, Italy*. ORCID: 0000-0001-9227-1059; Email: luca.muccioli@unibo.it

Benoît Champagne, *Unité de Chimie Physique Théorique et Structurale, Chemistry Department, Namur Institute of Structured Matter (NISM), University of Namur, Belgium*. ORCID: 0000-0003-3678-8875; Email: benoit.champagne@unamur.be

Notes

Biographies

Frédéric Castet is Professor in the Chemistry Department of the University Bordeaux (France). His research activities focus on the modeling of the electronic and (nonlinear) optical properties of molecular systems and materials with promising characteristics for exploitation in opto-electronics and photonic devices.

Claire Tonnelé is Junior Researcher at the Donostia International Physics Centre (DIPC, Spain). Her research activity lies in the computational study of organic (functional) materials to establish structure-property relationships and obtain a comprehensive picture of the underlying photophysical processes.

Luca Muccioli is Associate Professor of Physical Chemistry in the Industrial Chemistry Department of the University of Bologna (Italy). His main research activity deals with the application of computational chemistry techniques to the prediction of structural and electronic properties of materials, liquid crystals, and organic semiconductors, in particular through multiscale approaches.

Benoît Champagne is Professor in the Chemistry Department of the University of Namur (Belgium). His research activities tackle the development and application of quantum chemistry methods to predict and interpret electronic and (nonlinear) optical properties of molecules, polymers, surfaces, and crystals as well as their vibrational signatures.

References

[1] Pielak, K.; Tonnelé, C.; Sanguinet, L.; Cariati, E.; Righetto, S.; Muccioli, L.; Castet, F.; Champagne, B. Dynamical behavior and second harmonic generation responses in acido-triggered molecular switches. *J. Phys. Chem. C*. **2018**, *122*, 26160-26168.

[2] Tonnelé, C.; Champagne, B.; Muccioli, L.; Castet F. Nonlinear Optical Contrast in Azobenzene-Based Self-assembled Monolayers. *Chem. Mater*. **2019**, 31, 6759-6769.

[3] Bouquiaux, C.; Tonnelé, C.; Castet, F.; Champagne, B. Second-Order Nonlinear Optical Properties of an Amphiphilic Dye Embedded in a Lipid Bilayer. A Combined Molecular Dynamics - Quantum Chemistry Study. *J. Phys. Chem. B* **2020**, *124*, 2101-2109.

[4] L. Lescos, P. Beaujean, C. Tonnelé, P. Aurel, M. Blanchard-Desce, V. Rodriguez, M. de Wergifosse, B. Champagne, L. Muccioli, F. Castet Self-assembling, structure and nonlinear optical properties of fluorescent organic nanoparticles in water. *Phys. Chem. Chem. Phys*. **2021**, 23, 23643–23654.

[5] Maiman, T. H. Stimulated Optical Radiation in Ruby. *Nature* **1960**, *187*, 493-494.

[6] Franken, P. A.; Hill, A. E.; Peters, C. W.; Weinreich, G. Generation of Optical Harmonics. *Phys. Rev. Lett*. **1961**, *7*, 118-120.

[7] Shen, Y. R. Surface Properties Probed by Second-Harmonic and Sum-Frequency Generation. *Nature* **1989**, *337*, 519-525.

[8] Eisenthal, K. B. Liquid Interfaces Probed by Second-Harmonic and Sum-Frequency Spectroscopy. *Chem. Rev*. **1996**, *96*, 1343-1360.

[9] Dalton, L. R.; Sullivan, P. A.; Bale, D. H. Electric field poled organic electro-optic materials: state of the art and future prospects. *Chem. Rev*. **2010**, *110*, 25-55.

[10] Stegeman, G. I.; Stegeman, R. A. Nonlinear optics: phenomena, materials and devices. Hoboken, N. J.: John Wiley and Sons; **2012**.

[11] Sheppard, C.; Gannaway, J.; Kompfner, R.; Walsh, D. The scanning harmonic optical microscope. *IEEE J. Quantum Electron*. **1977**, *13*, 912.

[12] Freund, I.; Deutsch, M. Second-Harmonic Microscopy of Biological Tissue. *Opt. Lett.* **1986**, *11*, 94-96.

[13] Campagnola, P. J.; Wei M. D.; Loew, L. M.; High- Resolution Nonlinear Optical Imaging of Live Cells by Second Harmonic Generation. *Biophys. J*. **1999**, *77*, 3341-3349.

[14] Campagnola, P.; Loew, L. Second-harmonic imaging microscopy for visualizing biomolecular arrays in cells, tissues and organisms. *Nat. Biotechnol*. **2003**, *21*, 1356-1360.

[15] Kanis, D. R.; Ratner, M. A.; Marks, T. J. Design and construction of molecular assemblies with large second-order optical nonlinearities. Quantum chemical aspects. *Chem. Rev*. **1994**, *94*, 195-242.

[16] F. Castet, A. Gillet, F. Bureš, A. Plaquet, V. Rodriguez, B. Champagne Second-order nonlinear optical properties of Λ-shaped pyrazine derivatives. *Dyes and Pigments* **2021**, *184*, 108850.

[17] Brédas, J.-L.; Meyers, F.; Pierce, B. M.; Zyss, J. On the second-order polarizability of conjugated π-electron molecules with octupolar symmetry: the case of triaminotrinitrobenzene. *J. Am. Chem. Soc*. **1992**, *114*, 4928-4929.

[18] Kim, H. M.; Cho, B. R.; Second-order nonlinear optical properties of octupolar molecules structure–property relationship. *J. Mater. Chem*. **2009**, 19, 7402-7409.

[19] Castet, F.; Blanchard-Desce, M.; Adamietz, F.; Poronik, Y. M.; Gryko, D. T.; Rodriguez, V.; Experimental and Theoretical Investigation of the First-order Hyperpolarizability of Octupolar Merocyanines Dyes. *ChemPhysChem*. **2014**, *15*, 2575-2581.

[20] Coe, B. J. Molecular Materials Possessing Switchable Quadratic Nonlinear Optical Properties. *Chem. − Eur. J.* **1999**, *5*, 2464-2471.

[21] Delaire, J. A.; Nakatani, K. Linear and Nonlinear Optical Properties of Photochromic Molecules and Materials. *Chem. Rev*. **2000**, *100*, 1817-1845.

[22] Castet, F.; Rodriguez, V.; Pozzo, J.-L.; Ducasse, L.; Plaquet, A.; Champagne, B. Design and Characterization of Molecular Nonlinear Optical Switches. *Acc. Chem. Res*. **2013**, *46*, 2656-2665.

[23] Chen, K. J.; Laurent A. D.; Jacquemin, D. Strategies for Designing Diarylethenes as Efficient Nonlinear Optical Switches. *J. Phys. Chem. C* **2014**, *118*, 4334-4345.

[24] Jaunet-Lahary, T.; Chantzis, A.; Chen, K. J.; Laurent A. D.; D. Jacquemin, Designing Efficient Azobenzene and Azothiophene Nonlinear Optical Photochromes. *J. Phys. Chem. C* **2014**, *118*, 28831–28841

[25] Beaujean, P.; Bondu, F.; Plaquet, A.; Garcia-Amorós, J.; Cusido, J.; Raymo, F. M.; Castet, F.; Rodriguez, V.; Champagne, B. Oxazines: A New Class of Second-Order Nonlinear Optical Switches. *J. Am. Chem. Soc*. **2016**, *138*, 5052-5062.

[26] C. Tonnelé, B. Champagne, L. Muccioli and F. Castet, Second-order nonlinear optical properties of Stenhouse photoswitches: insights from density functional theory. *Phys. Chem. Chem. Phys*. **2018**, *20*, 27658-27667.

[27] Champagne, B.; Perpète, E. A.; Jacquemin, D.; van Gisbergen, S. J. A.; Baerends, E.-J.; Soubra-Ghaoui, C.; Robins, K. A.; Kirtman, B. Assessment of Conventional Density Functional Schemes for Computing the Dipole Moment and (Hyper)polarizabilities of Push-Pull π-Conjugated Systems. *J. Phys. Chem. A* **2000**, *104*, 4755-4763.

[28] Bulat, F. A.; Toro-Labbé, A.; Champagne, B.; Kirtman, B.; Yang, W. Density-functional theory (hyper)polarizabilities of push-pull p-conjugated systems: Treatment of exact exchange and role of correlation. *J. Chem. Phys.* **2005**, *123*, 014319.

[29] Jacquemin, D.; Perpète, E. A.; Medved', M.; Scalmani, G.; Frisch, M. J.; Kobayashi, R.; Adamo, C.; First Hyperpolarizability of Polymethineimine with Long-Range Corrected Functionals. *J. Chem. Phys.* **2007**, *126*, 191108.

[30] L. E. Johnson, L. R. Dalton and B. H. Robinson, Optimizing Calculations of Electronic Excitations and Relative Hyper- polarizabilities of Electrooptic Chromophores. *Acc. Chem. Res*. **2014**, *47*, 3258-3265.

[31] Zaleśny, R.; Medved', M.; Sitkiewicz, S. P.; Matito, E.; Luis, J. M.; Can Density Functional Theory Be Trusted for High-Order Electric Properties? The Case of Hydrogen-Bonded Complexes. *J. Chem. Theory Comput*. **2019** *15*, 3570-3579.

[32] Lescos, L.; Sitkiewicz, S. P.; Beaujean, P.; Blanchard-Desce, M.; Champagne, B.; Matito, E.; Castet, F. Performance of DFT Functionals for Calculating the Second-Order Nonlinear Optical Properties of Dipolar Merocyanines. *Phys. Chem. Chem. Phys*. **2020**, *22*, 16579-16594.

[33] C. Naim, F. Castet, E. Matito Impact of Van der Waals interactions on structural and nonlinear optical properties of azobenzene switches. *Phys. Chem. Chem. Phys*. **2021**, *23*, 21227-21239.

[34] Hendrickx, E.; Clays, K.; Persoons, A. Hyper-Rayleigh Scattering in Isotropic Solution. *Acc. Chem. Res.* **1998**, *31*, 675-683.

[35] Ledoux, I.; Zyss, J. Influence of the Molecular Environment in Solution Measurements of the Second-Order Optical Susceptibility for Urea and Derivatives. *Chem. Phys.* **1982**, 73, 203-213.

[36] The expressions for $\langle \beta_{ZZZ}^2 \rangle$, $\langle \beta_{ZXX}^2 \rangle$ $\gamma_{//}$, and $\beta_{//}$ in terms of molecular β and γ tensor components are provided in the Supporting Information (SI).

[37] Marazzini, G.; Giovannini, T.; Egidi, F.; Cappelli, G. Calculation of Linear and Non-linear Electric Response Properties of Systems in Aqueous Solution: A Polarizable Quantum/Classical Approach with Quantum Repulsion Effects. *J. Chem. Theory Comput.* **2020**, *16*, 6993−7004

[38] Helgaker, T.; Coriani, S.; Jørgensen, P.; Kristensen, K.; Olsen, J.; Ruud, K. Recent Advances in Wave Function-Based Methods of Molecular-Property Calculations. *Chem. Rev.* **2012**, *112*, 543-631.

[39] de Wergifosse, M.; Grimme, S. Perspective on Simplified Quantum Chemistry Methods for Excited States and Response Properties. *J. Phys. Chem. A* **2021**, *125*, 3841–3851.

[40] Pielak, K.; Bondu, F.; Sanguinet, L.; Rodriguez, V.; Champagne B.; Castet F. Second-order nonlinear optical properties of multi-addressable indolino-oxazolidine derivatives: Joint Computational and Hyper-Rayleigh Scattering Investigations. *J. Phys. Chem. C* **2017**, *121*, 1851-1860.

[41] Quentimont, J.; Champagne, B; Castet, F; Hidalgo Cardenuto, M. Explicit versus Implicit Solvation Effects on the First Hyperpolarizability of an Organic Biphotochrome. *J. Phys. Chem. A* **2015**, *119*, 5496-5503.

[42] Hidalgo Cardenuto, M.; Champagne, B. QM/MM investigation of the concentration effects on the second-order nonlinear optical responses of solutions. *J. Chem. Phys*. **2014**, *141*, 234104.

[43] Hidalgo Cardenuto, M.; Champagne, B. The first hyperpolarizability of nitrobenzene in benzene solutions: investigation of the effects of electron correlation within the sequential QM/MM approach. *Phys. Chem. Chem. Phys*. **2015**,*17*, 23634-23642.

[44] Giovannini, T.; Ambrosetti, M.; Cappelli, C. A polarizable embedding approach to second harmonic generation (SHG) of molecular systems in aqueous solutions. *Theor. Chem. Acc*. **2018**, *137*, 74.

[45] Hrivnák, T.; Reis, H.; Neogrády, P.; Zaleśny, R.; Medved', M. Accurate Nonlinear Optical Properties of Solvated para-Nitroaniline Predicted by an Electrostatic Discrete Local Field Approach. *J. Phys. Chem. B* **2020** *124*, 10195-10209

[46] Méreau, R.; Castet, F.; Botek, E.; Champagne B. Effect of the Dynamical Disorder on the Second-Order Nonlinear Optical Responses of Helicity-Encoded Polymer Strands. *J. Phys. Chem. A* **2009**, *113*, 6552.

[47] Seibert, J.; Champagne, B.; Grimme, S.; de Wergifosse, M. Dynamic Structural Effects on the Second-Harmonic Generation of Tryptophane-Rich Peptides and Gramicidin A. *J. Phys. Chem. B* **2020**, *124*, 2568-2578.

[48] Pracht, P.; Bohle, F.; Grimme, S. Automated exploration of the low-energy chemical space with fast quantum chemical methods. *Phys. Chem. Chem. Phys*. **2020**, *22*, 7169-7192.

[49] Kenis, P.J.A.; Noordman, O.F.J.; Houbrechts, S.; van Hummel, G.J.; Karkema, S., van Veggel, F.C.J.M.; Clays, K.; Engbersen, J.F.J.; Persoons, A.; van Hults, N.F.; Reinhoudt, D.N. Second-Order Nonlinear Optical Properties of the Four Tetranitrotetrapropoxycalix[4]arene Conformers. *J. Am. Chem. Soc*. **1998**, *120*, 7875-7883.

[50] Ramos, T. N.; Canuto, S.; Champagne, B. Unraveling the Electric Field-Induced Second Harmonic Generation Responses of Stilbazolium Ion Pairs Complexes in Solution Using a Multiscale Simulation Method. *J. Chem. Inf. Model*. **2020**, 60, 4817−4826.

[51] Ramos, T. N.; Castet, F.; Champagne B. Second Harmonic Generation Responses of Ion-Pairs Revealing the Formation of Dimeric Aggregates. *J. Phys. Chem. B* **2021**, 125, 3386−3397.

[52] Daniel, J.; Bondu, F.; Adamietz, F.; Blanchard-Desce, M.; Rodriguez, V. Interfacial organization in dipolar dye-based organic nanoparticles probed by second-harmonic scattering. *ACS Photon.* **2015**, 2, 1209–1216.

[53] Tonnelé, C.; Pielak, K.; Deviers, J.; Muccioli, L.; Champagne, B.; Castet, F. Nonlinear optical responses of self-assembled monolayers functionalized with indolino-oxazolidine photoswitches. *Phys. Chem. Chem. Phys*. **2018**, 20, 21590-21597.

[54] Schulze, M.; Utecht, M.; Moldt, T.; Przyrembel, D.; Gahl, C.; Weinelt, M.; Saalfrank, P.; Tegeder, P. Nonlinear optical response of photochromic azobenzene-functionalized self-assembled monolayers. *Phys. Chem. Chem. Phys*. **2015**, 17, 18079−18086.

[55] Bouquiaux, C.; Castet, F.; Champagne, B. Unravelling the Effects of Cholesterol on the Second-Order Nonlinear Optical Responses of Di-8-ANEPPS Dye Embedded in Phosphatidylcholine Lipid Bilayers. *J. Phys. Chem. B* **2021**, *125*, 10195-10212.

[56] Shelton, D.P. Hyper-Rayleigh Scattering from Correlated Molecules. *J. Chem. Phys.* **2013**, 138, 154502.

[57] Jung, K. A.; Videla, P. E.; Batista, V. S. Inclusion of nuclear quantum effects for simulations of nonlinear spectroscopy. *J. Chem. Phys.* **2018**, *148*, 244105.

[58] Makri, N. Quantum-classical path integral: A rigorous approach to condensed phase dynamics. *Int. J. Quantum Chem.* **2015**, *115*, 1209–1214.

[59] D'Avino, G.; Muccioli, L.; Castet, F.; Poelking, C.; Andrienko, D.; Soos, Z. G.; Cornil, J.; Beljonne, D. Electrostatic phenomena in organic semiconductors: fundamentals and implications for photovoltaics. *J. Phys.: Condens. Matter* **2016**, *28*, 433002.

[60] Seidler, T.; Krawczuk, A.; Champagne, B.; Stadnicka, K. QTAIM-Based Scheme for Describing the Linear and Nonlinear Optical Susceptibilities of Molecular Crystals Composed of Molecules with Complex Shapes. *J. Phys. Chem. C* **2016**, 120, 4481-4494.

[61] Zhou, Z.; Parker, S. M. Accelerating molecular property calculations with semiempirical preconditioning. *J. Chem. Phys.*, **2021**, 155, 204111.

[62] Kussmann, J.; Ochsenfeld, C. A Density Matrix-Based Method for the Linear-Scaling Calculation of Dynamic Second- and Third-Order Properties at the Hartree-Fock and Kohn-Sham Density Functional Theory Levels. *J. Chem. Phys.* **2008**, 127, 204103